Ultra-broadband absorption in mid-infrared spectrum with graded permittivity metamaterial waveguide structure

**Nan Zhang · Peiheng Zhou · Linbo Zhang ·
Xiaolong Weng · Jianliang Xie · Longjiang Deng**

Abstract   In this work, we demonstrate an ultra-broadband metamaterial absorber working in mid-infrared spectrum with a graded permittivity waveguide structure. The proposed absorber can achieve near-perfect absorption at wavelengths in the range from 3.4 to 5.8 μm. The absorption bandwidth is maintained quite well even at large angles of incidence. The gradually changing permittivity of the dielectric films in the multilayered absorber allows light capture through slow light mode and energy dissipation through localized electromagnetic resonance. The design approach presented here is effective for the construction of broadband absorbers and is also helpful as a theoretical support for the fabrication of other photonic devices.

1 Introduction

Artificial electromagnetic materials, including photonic crystals [1, 2], plasmonic structures [3], and metamaterials [4–6], have attracted considerable attention due to their unique ability to produce numerous exotic effects that are not obtainable in nature. These structures are able to manipulate light through use of their unit cell geometries and compositions. One currently burgeoning field of research is that of metamaterial perfect absorbers (MPAs) [7–10]. After first demonstration of the microwave MPA [7], research interest in this topic has grown rapidly, and extensive follow-up work has been carried out to make

absorbers wide-angle compatible and polarization insensitive [11–15]. However, the inherently resonant nature of metamaterials determines that the absorption bandwidths of MPAs are usually narrow, which limits their potential applications in many fields, such as high-efficiency solar cells and high-sensitivity photodetectors. A number of efforts have been made to extend the absorption bandwidth through the concept of multiresonances [16–19]. Multiresonant broadband absorbers are generally realized using an elaborate blend of dimensionally dispersed metallic resonators that are arranged either vertically or horizontally. Each resonator in the absorber resonates at a slightly different frequency to the other resonators, and the superposition of all these resonances results in broadband absorption. Randomly stacked gold nanorods have also demonstrated highly efficient broadband absorption in the 900–1,600 nm wavelength range [20]. The diversity of the gold nanorods and the multilayer configuration are major factors in the broadband absorption. The most extreme case of dimensional dispersion is that of anisotropic broadband absorbers [21–24], in which size-tapered waveguides were able to support the slow light mode, and the light can be absorbed over an unprecedentedly broad waveband. However, to date, almost all published research associated with bandwidth extension has focused on engineering of the metallic resonator geometry, while the important role of the constituent materials, and particularly the potential values of the dielectric spacers, has not been studied sufficiently.

In the field of antireflection (AR) coatings, multilayered films with graded permittivities have been used for broadband elimination of Fresnel reflection [25, 26]. The incident light penetrates into the coating films with given permittivities and enters the substrate without meeting any distinct optical interface that may cause reflection. However, this kind of AR coating apparently could not work

N. Zhang · P. Zhou (✉) · L. Zhang · X. Weng · J. Xie · L. Deng
National Engineering Research Center of Electromagnetic
Radiation Control Materials, State Key Laboratory of Electronic
Thin Film and Integrated Devices, University of Electronic
Science and Technology of China, Chengdu 610054, China
e-mail: phzhou@uestc.edu.cn

Fig. 1 Schematic view of the proposed absorber: **a** the periodic arrangement; **b** the geometry of a single unit cell
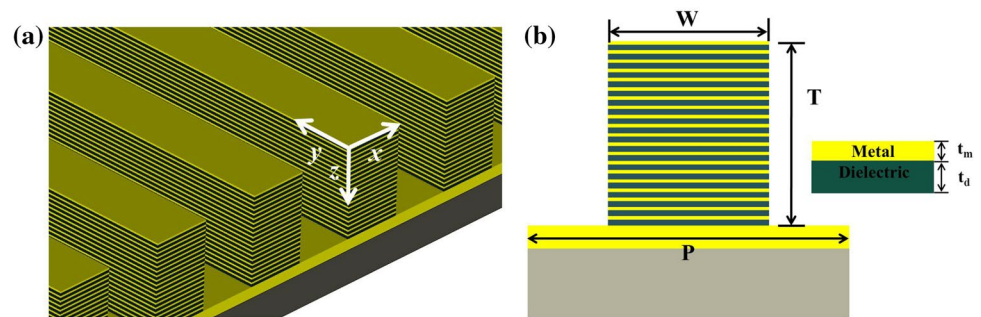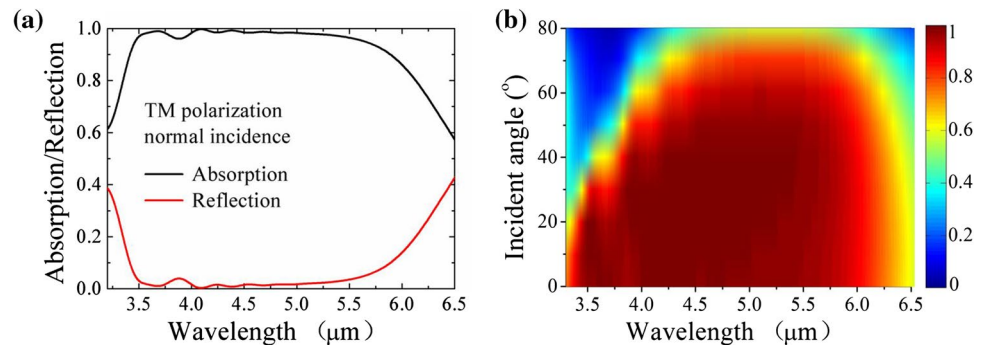

Fig. 2 **a** Absorption and reflection spectra of the proposed absorber for light at normal incidence. **b** Angular dispersion of the absorption spectra

as a broadband absorber because of the high transmission of the structure. In this letter, by approaching the problem from another perspective, we demonstrate an absorber constructed of idealized dielectric films with graded relative permittivities in a multilayered MPA structure. The incident light is captured by vertically stacked metal/dielectric/metal resonant stacks that work as a group of slow light waveguides, and the energy is dissipated in association with the excitation of localized electromagnetic resonance. The proposed structure can significantly enhance absorption and reduce reflection over an ultra-broad spectral range. Unlike the structures of previous studies [16–19, 21–24], the broadband absorption of this structure is tuned by the permittivity of the constituent dielectric film rather than the morphology or the arrangement of the metallic resonator.

2 Structure design and simulation setup

Figure 1 illustrates the schematic view of the proposed absorber. The structure consists of alternating layers of metal and dielectric thin films stacked on a bottom metallic mirror. The total number of metal/dielectric pairs (N) is 20, and the constituent metal/dielectric thin films are carved into one-dimensional periodic slits. All the metal thin films are made of aluminum, and the dielectric thin films are made of distinct materials with relative permittivities that taper linearly (the tuning difference between adjacent dielectric spacers is $\Delta \varepsilon = 0.5$) from the bottom ($\varepsilon_b = 11.5$) to

the top ($\varepsilon_t = 2$). The absorber has geometrical parameters of $P = 1,400$ nm, $W = 700$ nm, $T = 800$ nm, $t_m = 15$ nm, and $t_d = 25$ nm, as shown in Fig. 1b. Numerical simulations were performed using a finite-difference time-domain (FDTD) algorithm [27] to investigate the resonant behavior of the proposed structure. In the simulations, the dielectric film is set to be lossless, and the complex permittivity of Al is described by the Drude model with plasma frequency $\omega_p = 2\pi \times 2,895$ THz and collision frequency $\omega_\gamma = 2\pi \times 15.5$ THz [28]. Periodic boundary conditions were employed for the x–y plane, and a plane wave with TM polarization (magnetic field H perpendicular to the x–z plane) representing the excitation source was normally incident upon the structure. The frequency-dependent absorption was obtained from the S-parameters by $A(\omega) = 1 - T(\omega) - R(\omega) = 1 - |S_{21}|^2 - |S_{11}|^2$, where $T(\omega)$ and $R(\omega)$ are the frequency-dependent transmission and reflection, respectively. Because the 100-nm-thick bottom metallic mirror (the continuous Al film) is thick enough to suppress all light transmission ($T(\omega) = 0$), the absorption calculation could then be simplified to $A(\omega) = 1 - R(\omega)$. In this case, the broadband perfect absorber also acts as a broadband perfect antireflector.

3 Results and discussion

The calculated absorption and reflection spectra of the proposed absorber for normal incidence are shown in Fig. 2a.

Fig. 3 Distributions of the electric field (*top row*), the magnetic field (*middle row*), and the energy flow (*bottom row*) in the x–z plane of the proposed absorber for three different wavelengths: **a**, **d**, and **g** are for $\lambda_0 = 3.7$ μm; **b**, **e**, and **h** are for $\lambda_0 = 4.7$ μm; and **c**, **f**, and **i** are for $\lambda_0 = 5.7$ μm. The incident plane wave is normal to the absorber and is absorbed as shown in Fig. 2a
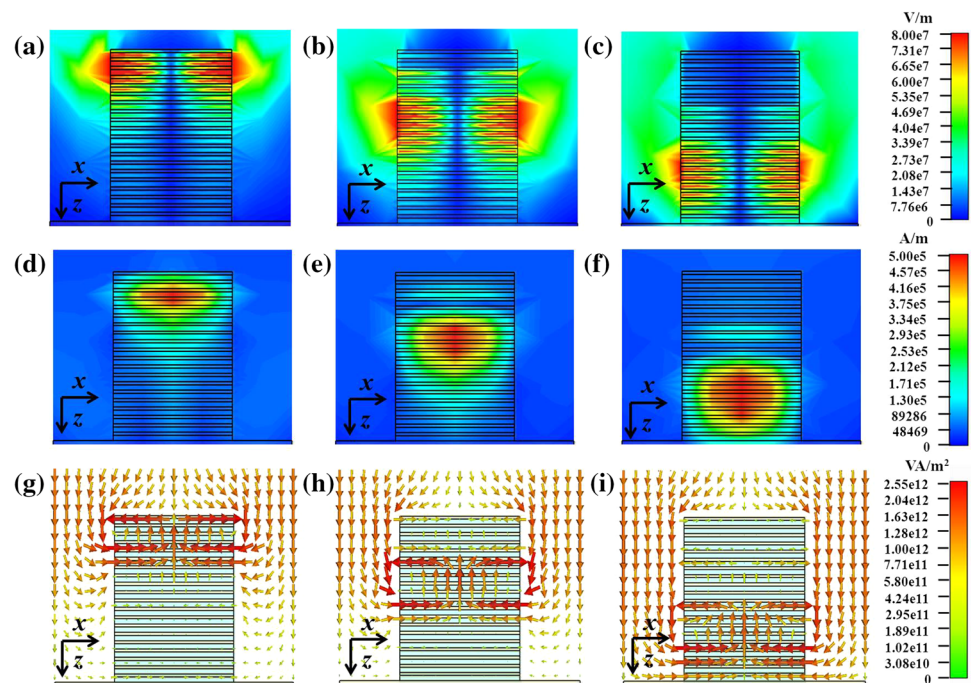
Near-perfect absorption and near-zero reflection are achieved in the 3.4–5.8 μm wavelength range. This means that the incident light is almost entirely absorbed by the absorber, with no reflection within the waveband. Since the absorption bandwidth of single band MPAs is relatively narrow at typically no more than 20 % of the center frequency, the proposed absorber exhibits excellent broadband absorption performance. Also, the absorption bandwidth of the proposed absorber is superior to that of the dimensionally dispersed broadband absorber [18, 19] and comparable to that of the size-tapered slow light broadband absorber [21]. Further simulations were carried out to evaluate the absorption performance of this structure for light at oblique angles of incidence. Figure 2b presents the angular dispersion of the absorption spectra. The broadband absorption characteristics are maintained quite well with increasing incident angle, and the bandwidth of 80 % absorptivity is retained up to 1.7 μm, even at an angle of incidence of 60°.

To understand the broadband absorption mechanism, the electric field and magnetic field distributions in the structure were observed at three different wavelengths. The wavelengths of 3.7, 4.7, and 5.7 μm represent the initial, middle, and end stages of the near-perfect absorption part of the absorption spectrum shown in Fig. 2a. As illustrated in Fig. 3, the enhanced electromagnetic fields are resonantly excited at specific parts of the absorber. For resonance at the short wavelength, $\lambda_0 = 3.7$ μm (Fig. 3a, d), the energy is gathered at the upper part of the absorber, where the permittivities of the dielectric films are relatively small. However, for resonance at the long wavelength,

$\lambda_0 = 5.7$ μm (Fig. 3c, f), the energy is trapped in the lower part of the absorber, where the dielectric films have relatively large permittivities. Correspondingly, for the resonance at the middle of the absorption band at $\lambda_0 = 4.7$ μm (Fig. 3b, e), the energy is harvested from the middle part of the absorber. These phenomena are primarily associated with the excitation of localized electric and magnetic dipole resonances [9, 22]. Moreover, because the metal film thickness (t_m) is smaller than the skin depth of the metal within the frequency range under study, the enhanced electromagnetic field is not confined in the dielectric layer between two neighboring metal thin films, but diffuses into several nearby metal/dielectric layers. The diffusion effect indicates that the resonance in the absorber can be regarded as a hybrid mode that is supported by several adjacent resonant stacks [16].

Further understanding of the electromagnetic physics can be explained as follows (using the absorption at wavelength $\lambda_0 = 4.7$ μm as an example). As shown in Figs. 3b and 4a, b, the enhanced electric field concentrates at both the lateral edges of the stacks and the air gaps between two adjacent unit cells. This is the evidence of the existence of a strong electric dipole resonance, which is caused by localized surface plasmon polaritons excited at the metal/dielectric interface; thus, the charges are accumulated, and the localized electric field is enhanced [22, 29]. Meanwhile, the accumulated charges couple to their image charges on neighboring metal films in anti-phase (Fig. 4b). Consequently, magnetic polaritons are formed, and magnetic dipole resonance is generated between the neighboring

Fig. 4 Distributions of (**a**) *z*-component of the electric field at the metal/dielectric interface (height $t = T/2 = 400$ nm); **b** *z*-component of the electric field; **c** *y*-component of the magnetic field; and **d** energy dissipation of the proposed one-dimensional absorber. The chosen absorption wavelength was $\lambda_0 = 4.7$ μm
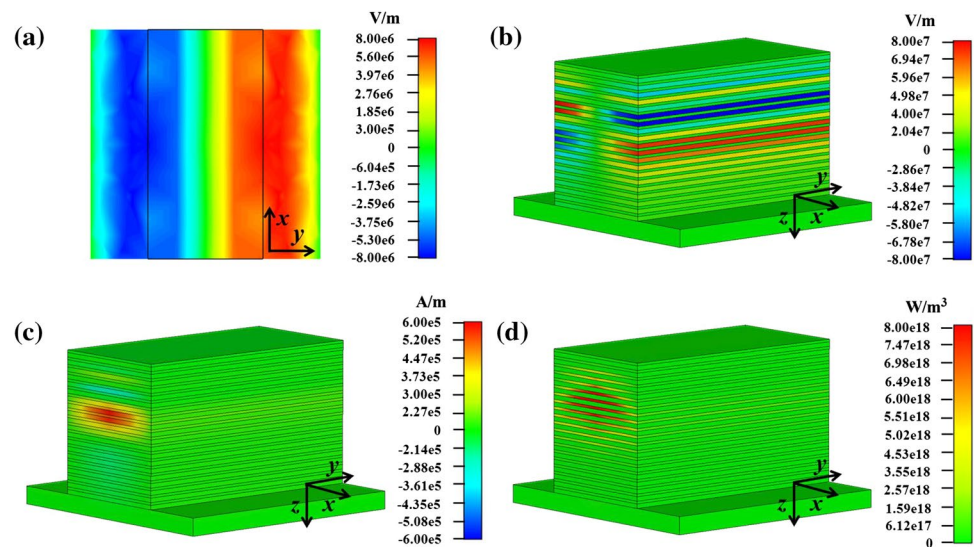
metal layers along the *y*-axis (Fig. 4c) [16, 22]. This strong electric resonance and magnetic resonance can couple efficiently to the incident light and dissipate the energy via ohmic losses within the metals (Fig. 4d), because the dielectric films are lossless [9]. In addition, the localized surface plasmon resonance wavelength increases linearly as the permittivity of the dielectric film increases [30]. In other words, a larger dielectric film permittivity produces a correspondingly smaller resonance frequency. Therefore, the proposed graded permittivity absorber can support the effective resonances over a wide frequency range, and thus, the collection of these resonances results in ultra-broadband absorption.

Plots of the Poynting vectors (S) (Fig. 3g, h, i) provide another physical image of the light absorption process. As shown in Fig. 3g, h, i, the incoming energy first propagates in the air gaps along the *z*-axis without penetrating into the structure until it reaches the position where the enhanced electromagnetic field is concentrated, and then the energy whirls into the stacks. Light propagation in this manner has already been demonstrated in the air–dielectric–metal slow light waveguide [31] and has been used to capture optical energy [22, 25]. Similarly, our broadband absorber also uses this slow light trapping mechanism to trap and harvest light. To further explore the nature of the slow light operated in the absorber, we investigated a non-gradient structure with the same geometrical parameters as that shown in Fig. 1, while the permittivity of all the dielectric films was fixed at a constant value (i.e., $\Delta \varepsilon = 0$). According to effective medium theory, this stack of alternating layers of metal/dielectric thin films can be regarded as a homogeneous material with anisotropic permittivities that were described as follows [32]: $\varepsilon_{//} = f\varepsilon_{\mathrm{m}}(\omega) + (1 - f)\varepsilon_{\mathrm{d}}$, and $1/\varepsilon_{\perp} = f/\varepsilon_{\mathrm{m}}(\omega) + (1 - f)/\varepsilon_{\mathrm{d}}$, where $f = t_{\mathrm{m}}/(t_{\mathrm{m}} + t_{\mathrm{d}})$ is the filling ratio of the metal film. Then, the dispersion relation

between the incident photon frequency ($\omega_{\mathrm{c}} = \omega/c$) and the propagation constant (β) of this waveguide can be calculated by solving the eigenequation of the Bloch mode [33]:

$$\frac{\exp(-i\gamma_2 w) - \exp[\gamma_1(P - w)]}{\exp(i\gamma_2 w) - \exp[\gamma_1(P - w)]} = \left(\frac{\gamma_2\varepsilon_1 + i\gamma_1\varepsilon_{\perp}}{\gamma_2\varepsilon_1 - i\gamma_1\varepsilon_{\perp}}\right)^2 \frac{\exp(-i\gamma_2 w) - \exp[-\gamma_1(P - w)]}{\exp(i\gamma_2 w) - \exp[-\gamma_1(P - w)]}.$$

(1)

here, $\gamma_1 = (\beta^2 - \omega_{\mathrm{c}}^2\varepsilon_1)^{1/2}$, $\gamma_2 = (\omega_{\mathrm{c}}^2\varepsilon_{\perp} - \varepsilon_{\perp}\beta^2/\varepsilon_{//})^{1/2}$, and ε_1 is the relative permittivity of air.

The dispersion curves of the Bloch mode for the proposed effective homogeneous waveguides are shown in Fig. 5a. When we consider the alternating metal/dielectric structure, the propagation characteristics of these waveguides are strongly confined by the permittivities of the dielectric films. In our calculations, the values of the permittivities were chosen to be $\varepsilon_{\mathrm{d}} = 3, 5, 7, 9$ and 11. We can see that the cutoff frequency (f_{c}) is located at different positions for the different waveguides. For instance, when the waveguide is made of dielectric films with $\varepsilon_{\mathrm{d}} = 7$, f_{c} is approximately 57.7 THz, and the so-called slow light mode is generated at this frequency accordingly [22]. The wavelengths of the slow light mode (λ_{c}) that were obtained from the dispersion curves are shown in Fig. 5b. λ_{c} was found to increase linearly with increasing ε_{d}, and the slow light mode can be supported in the wavelength range from 3.3 to 6.5 μm, with ε_{d} varying from 2 to 11. Therefore, the proposed absorber, with ε_{d} tapering linearly from the bottom ($\varepsilon_{\mathrm{b}} = 11.5$) to the top ($\varepsilon_{\mathrm{t}} = 2$), can be regarded as a structure that is composed of a number of vertically stacked waveguides with graded permittivities (both $\varepsilon_{//}$ and $\varepsilon_{\perp}$). As a result, light in the 3.3–6.5 μm waveband incident upon the structure would be trapped in the absorber by the collective

Fig. 5 **a** Dispersion curves of the effective waveguides for various constituent dielectric films. **b** *Red hollow square dots* represent the cutoff wavelengths extracted from the dispersion curves; *black solid circular dots* represent the dielectric film permittivity at the energy center, as plotted in Fig. 3 for the absorption wavelength $\lambda = \lambda_c$
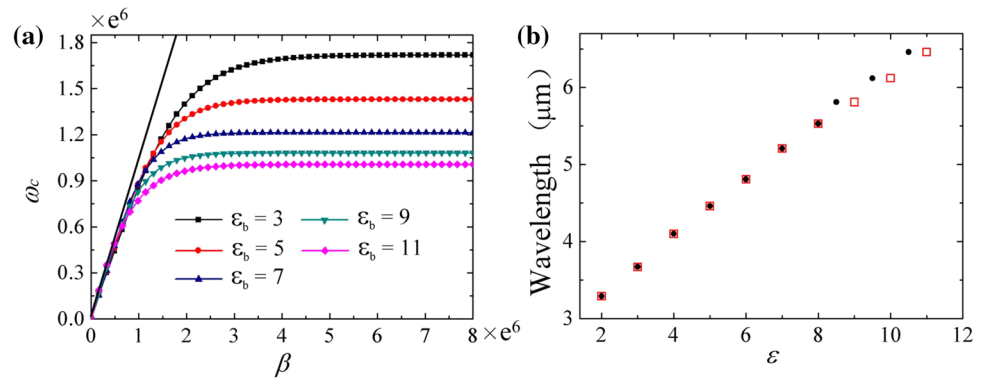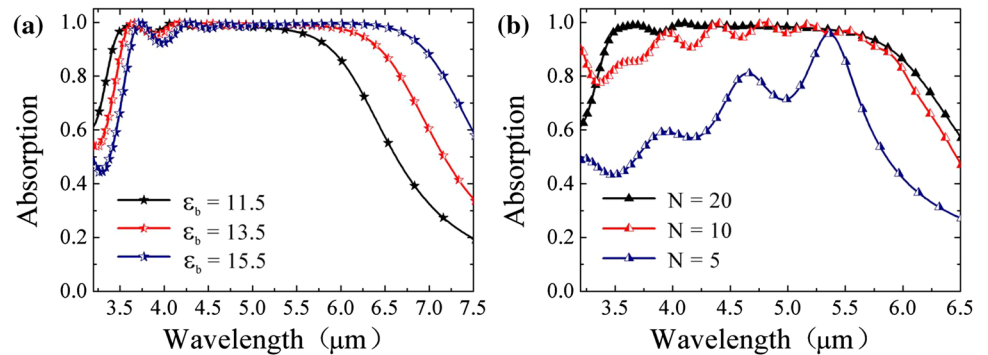

Fig. 6 Influence of the ε_d distribution on the absorption performance. **a** Simulated absorption spectra for $\varepsilon_b = 11.5$, 13.5, and 15.5, with all geometrical parameters and the top layer permittivity ($\varepsilon_t = 2$) fixed; **b** simulated absorption spectra for $N = 5$, 10, and 20 with $T = 800$ nm, $f = t_m/(t_m + t_d) = 0.375$, $\varepsilon_t = 2$, and $\varepsilon_b = 11.5$

effect of all these waveguides working together. Simultaneously, the trapped light excites both the electric and magnetic dipole resonances, as described above. The relationship between the slow light waves and the electromagnetic resonances can be confirmed further by extraction of the permittivity of the dielectric film at the energy center (similar to the three wavelengths used as examples in Fig. 3) for the absorption wavelength $\lambda = \lambda_c$. As shown in Fig. 5b, the electric and magnetic dipole resonances that are excited in the absorber are located exactly at the waveguides that have a slow light mode at the corresponding wavelength, except for those close to the bottom of the structure. The deviation between them is rooted in the simplification used for the dispersion calculation by converting the graded permittivity structure into a non-gradient structure, along with the additional impact from the bottom metallic mirror.

Thus, given the discussions presented above, we can determine that the excellent broadband absorption performance of the proposed absorber results from its graded permittivity profile, which allows effective light trapping and dissipation. The short metal/dielectric/metal waveguide with its fixed dielectric permittivity offers light guiding properties below the cutoff frequency (Fig. 5a), while the light that is guided into the structure would be trapped at a certain absorber position above the cutoff frequency for excitation of the slow light mode. The light trapped in the absorber would interact with the free electrons in the

metals in terms of localized electromagnetic resonances, and the energy would be finally dissipated as ohmic losses. The graded permittivity profile of the absorber can support the slow light mode and localized electromagnetic resonance over a broad waveband, and thus, ultra-broad absorption with excellent absorptivity can be achieved.

Since the ultra-broadband absorption is the tuning result of the constituent dielectric spacers, we then investigate the influence of the distribution of ε_d on the absorption performance. As discussed above, long wavelength incident light is trapped at the lower part of the absorber, where the dielectric film permittivity is large. Thus, the end wavelength of the absorption band is determined by ε_b when all the geometrical parameters and the top layer permittivity ($\varepsilon_t = 2$) are fixed. Figure 6a shows the simulated absorption spectra for $\varepsilon_b = 11.5$, 13.5, and 15.5. We see that as ε_b increases, the end wavelength of the absorption band also increases, but the initial wavelength of the absorption band remains almost fixed. Therefore, an increase in the absorption bandwidth is introduced. Also, with increasing ε_b, the oscillation of the absorption spectra becomes increasingly strong and undesirable small dips emerge. This behavior is attributed to the increase in $\Delta\varepsilon$ over the entire structure rather than the change in the material parameters in the dielectric layers. Because the frequency difference derived from adjacent resonant stacks is enlarged in this case, the coupling or the continuity between the neighboring

resonant wavelengths deteriorates. Similarly, the initial wavelength of the absorption band can be tuned by ε_t with the end wavelength of the absorption band is fixed (not shown here).

However, if we suppose that ε_d is varied within a given numerical range, then the permittivity gradient in the proposed absorber is determined by the number of metal/dielectric pairs (N). For $T = 800$ nm, $f = t_m/(t_m + t_d) = 0.375$, $\varepsilon_t = 2$, and $\varepsilon_b = 11.5$, Fig. 6b illustrates the absorption spectra of absorbers with $N = 5$, 10, and 20. When compared with $N = 20$ ($\Delta\varepsilon = 0.5$), the absorption spectrum for $N = 10$ ($\Delta\varepsilon = 1.06$) is degraded over the entire absorption band with distinguishable oscillations and deep dips. A further reduction in the number of metal/dielectric pairs to $N = 5$ ($\Delta\varepsilon = 2.38$) induces serious shrinkage in the resonance numbers and separation of the remaining resonances, and thus, the continuous broadband absorption spectrum cannot be retained. Also, when $N = 5$, the metal films are very thick, and thus, the effective medium theory is not valid anymore. However, the absorption bandwidth of 70 % absorptivity is still available up to 1.2 μm in this case, which is better than the designs described in [24] with comparatively fewer tapered resonant stacks. Therefore, for the proposed graded permittivity absorber, an appropriate $\Delta\varepsilon$ value is of critical importance to ensure that the absorption band is both broad and flat.

For experimental realization of this ultra-broadband absorber, standard ultraviolet lithography and physical vapor deposition techniques can be used to fabricate the optimized device. Because all the resonant stacks have the same geometrical dimensions in the x–y plane, the lithography step need only to be performed once to define the structure, and then the alternately deposited dielectric and metallic films can be shaped by the patterned photoresist. Dielectric films with graded permittivities can be achieved by using oblique-angle deposition [26]. The permittivity of the dielectric film can be varied controllably over a certain range by changing the incident vapor angle. Therefore, if we elaborately select the dielectric materials (e.g., Ge, ZnSe, ZnS, Al_2O_3, SiO_2, and MgF_2) and control the angles of incidence of their vapors, then the permittivity of the dielectric film can be varied continuously over quite a wide range. In addition, although the absorber presented here can only absorb TM-polarized incident light, it could also easily be made to work as a polarization-independent absorber by curving the surface into symmetrical structures (e.g., circles or squares).

4 Conclusions

In conclusions, we have demonstrated an ultra-broadband metamaterial absorber for the mid-infrared spectrum that can efficiently absorb incident light over a wide waveband, even at large angles of incidence. The graded permittivity profile of the absorber offers ultra-broad absorption and permits engineering of the absorption spectrum. Achieving broadband absorption by tuning of the permittivity of the constituent dielectric films rather than the metallic resonator provides another degree of freedom to construct broadband MPAs, which may be useful in cases that the geometrical parameters of the absorber cannot be easily varied when it is integrated with other devices. The dimensional uniformity of the resonant stacks in the transverse plane makes that the entire structure can be shaped by just a single lithographic step, which will simplify the nano-fabrication process. The design approach presented here also has multiple application values in relevant fields that include high-sensitivity detection, energy harvesting, and thermal modulation.

References

1. J.D. Joannopoulos, P.R. Villeneuve, S. Fan, Nature **386**, 143 (1997)
2. J.D. Joannopoulos, S.G. Johnson, J.N. Winn, R.D. Meade, *Photonic crystals: molding the flow of light* (Princeton university press, Princeton, 2011)
3. S.A. Maier, *Plasmonics: fundamentals and applications* (Springer, Berlin, 2007)
4. D.R. Smith, J.B. Pendry, M.C.K. Wiltshire, Science **305**, 788 (2004)
5. D. Schurig, J.J. Mock, B.J. Justice, S.A. Cummer, J.B. Pendry, A.F. Starr, D.R. Smith, Science **314**, 977 (2006)
6. N. Engheta, R.W. Ziolkowski, *Metamaterials: physics and engineering explorations* (Wiley, New York, 2006)
7. N.I. Landy, S. Sajuyigbe, J.J. Mock, D.R. Smith, W.J. Padilla, Phys. Rev. Let. **100**, 207402 (2008)
8. X. Liu, T. Starr, A.F. Starr, W.J. Padilla, Phys. Rev. Lett. **104**, 207403 (2010)
9. J. Hao, J. Wang, X. Liu, W.J. Padilla, L. Zhou, M. Qiu, Appl. Phys. Lett. **96**, 251104 (2010)
10. N. Liu, M. Mesch, T. Weiss, M. Hentschel, H. Giessen, Nano Lett. **10**, 2342 (2010)
11. H. Tao, C.M. Bingham, A.C. Strikwerda, D. Pilon, D. Shrekenhamer, N.I. Landy, K. Fan, X. Zhang, W.J. Padilla, R.D. Averitt, Phys. Rev. B **78**, 241103 (R) (2008)
12. Y. Avitzour, Y.A. Urzhumov, G. Shvetset, Phys. Rev. B **79**, 045131 (2009)
13. A. Tittl, M.G. Harats, R. Walter, X. Yin, M. Schäferling, N. Liu, R. Rapaport, H. Giessen, ACS Nano **8**, 10885 (2014)
14. J. Grant, Y. Ma, S. Saha, L.B. Lok, A. Khalid, D.R.S. Cumming, Opt. Lett. **36**, 1524 (2011)
15. D. Cheng, J. Xie, H. Zhang, C. Wang, N. Zhang, L. Deng, J. Opt. Soc. Am. B **29**, 1503 (2012)
16. Y.Q. Ye, Y. Jin, S. He, J. Opt. Soc. Am. B **27**, 498 (2010)
17. J. Grant, Y. Ma, S. Saha, A. Khalid, D.R.S. Cumming, Opt. Lett. **36**, 3476 (2011)
18. S. Chen, H. Cheng, H. Yang, J. Li, X. Duan, C. Gu, J. Tian, Appl. Phys. Lett. **99**, 253104 (2011)

19. C. Cheng, M.N. Abbas, C. Chiu, K. Lai, M. Shih, Y. Chang, Opt. Express **20**, 10376 (2012)
20. X. Chen, H. Gong, S. Dai, D. Zhao, Y. Yang, Q. Li, M. Qiu, Opt. Lett. **38**, 2247 (2013)
21. Y. Cui, K.H. Fung, J. Xu, H. Ma, Y. Jin, S. He, N.X. Fang, Nano Lett. **12**, 1443 (2012)
22. Q. Liang, T. Wang, Z. Lu, Q. Sun, Y. Fu, W. Yu, Adv. Opt. Mater. **1**, 43 (2013)
23. J. Zhou, A.F. Kaplan, L. Chen, L.J. Guo, ACS Photonics **1**, 618 (2014)
24. D. Ji, H. Song, X. Zeng, H. Hu, K. Liu, N. Zhang, Q. Gan, Sci. Rep. **4**, 4498 (2014)
25. J.A. Dobrowolski, D. Poitras, P. Ma, H. Vakil, M. Acree, Appl. Opt. **41**, 3075 (2002)
26. J. Xi, M.F. Schubert, J.K. Kim, E.F. Schubert, M. Chen, S. Chen, S. Lin, W. Liu, J.A. Smart, Nat. Photonics **1**, 176 (2007)
27. CST Microwave Studio 2010, CST GmbH, Germany
28. M.A. Ordal, L.L. Long, R.J. Bell, S.E. Bell, R.R. Bell, R.W. Alexander Jr, C.A. Ward, Appl. Opt. **22**, 1099 (1983)
29. H. Raether, *Surface plasmons on smooth surface* (Springer, Berlin, 1988)
30. G. Lévêque, O.J.F. Martin, Opt. Lett. **31**, 2750 (2006)
31. J. He, S. He, IEEE Microw. Wirel. Compon. Lett. **16**, 96 (2006)
32. T.C. Choy, *Effective medium theory: principles and applications* (Oxford University Press, Oxford, 1999)
33. H. Hu, D. Ji, X. Zeng, K. Liu, Q. Gan, Sci. Rep. **3**, 1249 (2013)